

P1.3 ANALYSIS OF WIND STRESS ALGORITHMS AND COMPUTATION OF THE WIND STRESS CURL IN BODEGA BAY, CALIFORNIA

Adam Kochanski* and Darko Koracin

Desert Research Institute, Reno, Nevada

Clive E. Dorman

Scripps Institution of Oceanography and San Diego State University, San Diego, California.

1. INTRODUCTION

Difficulties in obtaining direct wind stress data cause, in many cases, the wind stress to be computed from bulk formulas that estimate turbulent fluxes on the basis of standard meteorological data. Since this approach to the wind stress evaluation is used in climate and ocean modeling, the goal of the presented work was to compare various wind stress formulas, and to estimate to what extent the choice of method alters the computed wind stress and wind stress curl.

Three commonly used algorithms of various complexities have been examined. As an example of the traditional scheme, we chose the Large and Pond (1981) formula (LP), that relates the drag coefficient (and consequently also the wind stress) only to the wind speed. The second scheme analyzed was the Hellerman and Rosenstein (1983) formula (HR), which for estimation of drag coefficient takes into account not only the wind speed, but also stability represented as the difference between the sea and air temperature. The most advanced of the analyzed schemes was the TOGA Coare algorithm (TC), taking into account the complexity of surface processes and computing the wind stress on the basis of surface fluxes analysis (Fairall et al. 1996 a,b).

2. ANALYZED WIND STRESS ALGORITHMS

2.1 Large and Pond (1981)

Large and Pond (1981) developed a simple algorithm consisting of a bulk formula for calculating the drag coefficient using only the wind velocity:

$$C_{D,LP} = 1.2 \cdot 10^{-3}, \quad \text{for } 4 \leq \bar{V} < 11 \text{ m s}^{-1} \quad (1)$$
$$C_{D,LP} = (0.49 + 0.065 \bar{V}) \cdot 10^{-3}, \quad \text{for } 11 \leq \bar{V} \leq 25 \text{ m s}^{-1}$$

where \bar{V} is the absolute value of the wind velocity, and $C_{D,LP}$ is the drag coefficient. This algorithm has been used in many studies such as Dorman et al. (2000), Samelson et al. (2002), and Koracin et al. (2004).

2.2 Hellerman and Rosenstein (1983)

The next level of complexity in calculating the drag coefficient, and subsequently the wind stress, is to include the air-sea temperature difference in addition to the wind velocity. This approach gives a relatively simple formula for drag coefficient calculation, which also takes into account a simplified treatment of stability conditions. As a consequence, the Hellerman and Rosenstein formula has been widely used in many oceanic models such as: the Geophysical Fluid Dynamics Laboratory-Modular Ocean Model 'GFDL-MON' (Roussenov et al. 1995), the Oceanic Component Model of Flexible Global Climate 'FGCM0' (Jin et al. 1999), and the Naval Research Laboratory's Layered Ocean Model 'NLOM' (Metzger 2003). According to the Hellerman and Rosenstein formula the drag coefficient is calculated as:

$$C_{D,HR} = \alpha_1 + \alpha_2 \bar{V} + \alpha_3 (T_a - T_s) + \alpha_4 \bar{V}^2 + \alpha_5 (T_a - T_s)^2 + \alpha_6 \bar{V} (T_a - T_s)^2 \quad (2)$$

where \bar{V} is the absolute value of the wind velocity, T_a and T_s are the temperatures of the air and sea respectively, and $[\alpha_1, \dots, \alpha_6]$ are constants $[0.934 \times 10^{-3}, 0.788 \times 10^{-4}, 0.868 \times 10^{-4}, -0.616 \times 10^{-6}, -0.120 \times 10^{-5}, \text{ and } -0.214 \times 10^{-5}]$.

2.3 TOGA Coare algorithm

Fairall et al. (1996a,b) developed a comprehensive algorithm for the wind stress computation, which takes into account dynamical and thermodynamical processes. The drag coefficient appears to be a complex function of the wind velocity, air temperature, SST, humidity, atmospheric pressure, shortwave and longwave radiation fluxes, and the height of the atmospheric boundary layer. The algorithm computes transfer coefficients for the momentum, heat and humidity on the basis of an iterative estimation of the scaling parameters and stability functions, according to the similarity theory.

3. METHODOLOGY

3.1 Field program

As a part of the NSF-sponsored Coastal Ocean Processes (CoOP) program, the Wind Events and Shelf Transport (WEST) study was conducted in northern California. A comprehensive field program including

*Corresponding author address:

Adam Kochanski, DRI, Division of Atmospheric Sciences,
2215 Raggio Parkway, Reno, NV 89512
e-mail: Adam.Kochanski@dri.edu

meteorological, and marine biology measurements was carried out over the shelf of Bodega Bay during 2001 and 2002. A special set of 5 buoys (see Fig.1), provided detailed measurements of wind speed and direction, air and sea surface temperature, humidity, and the longwave and shortwave radiation fluxes. On the basis of these, as well as additional National Data Buoy Center (NDBC) buoy data, an analysis of the computed wind stress and wind stress curl has been performed.

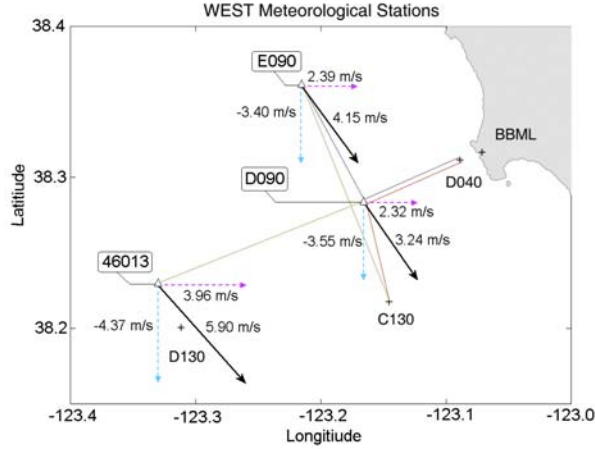


Fig. 1. Position of measurement buoys in Bodega Bay CA.

3.2 Wind stress analysis

A comparison of the wind stress computed from the three selected schemes has been performed using data from the central buoy D090 for the period from 28 June to 4 August 2001 (see Fig. 1). In order to investigate the effect of the broader range of the wind speed on the mean drag coefficient, calculations were performed also for three NDBC buoys - 46023, 46054 and 46062 - exposed to higher wind speeds during the same period. These buoys provided wind speed components, humidity and air and sea-surface temperatures. The longwave and shortwave radiation fluxes (required by the TC algorithm), were computed using the Bignami (1995) and Rosati and Miyakoda (1999) formulas.

In order to separate the influence of the wind speed from the influence of the temperature, humidity and other parameters, at the first step, all drag coefficients were computed under the neutral stability assumption (the same temperature of the air and the sea-surface). In this case, the Hellerman and Rosenstein formula (Eq. 2) reduces to the following:

$$C_{DN,HR} = \alpha_1 + \alpha_2 \bar{V} + \alpha_4 \bar{V}^2 \quad (3)$$

In order to obtain the neutral drag coefficient from the TOGA Coare algorithm, the friction velocity and the roughness length were calculated with the stability correction function equal to zero.

3.3 Analysis of the wind stress curl

For the wind stress curl computation, the triangle formation of buoys D090, E090 and 46013 was used (see Fig. 1). This setup allowed to estimate directly the wind stress curl, using the spatial variation of the wind stress computed from the buoy data. The buoy measurements included wind speed components, air and sea surface temperatures, radiation fluxes, and humidity. On the basis of this data, for each of the analyzed buoys, the west-east and south-north wind stress components τ_x and τ_y were computed. The wind stress curl for a given wind stress scheme was computed from the following equation:

$$Curl = \frac{\Delta \tau_y}{\Delta x} - \frac{\Delta \tau_x}{\Delta y} \quad (4)$$

where: $\Delta \tau_y = \tau_{\text{south-north,D090}} - \tau_{\text{south-north,E090}}$
 $\Delta \tau_x = \tau_{\text{west-east,D090}} - \tau_{\text{west-east,46013}}$
 Δx – west-east distance between buoys D090 and E90
 Δy – south-north distance between buoys D090 and 46013

4. RESULTS

4.1 Differences between the drag coefficient and the wind stress, computed using various schemes

Data for the period from 28 June to 4 August 2001 was used for computations of the drag coefficient and the wind stress. The drag coefficients computed from the three analyzed schemes using data from buoy D090 are shown in Fig.2a,b.

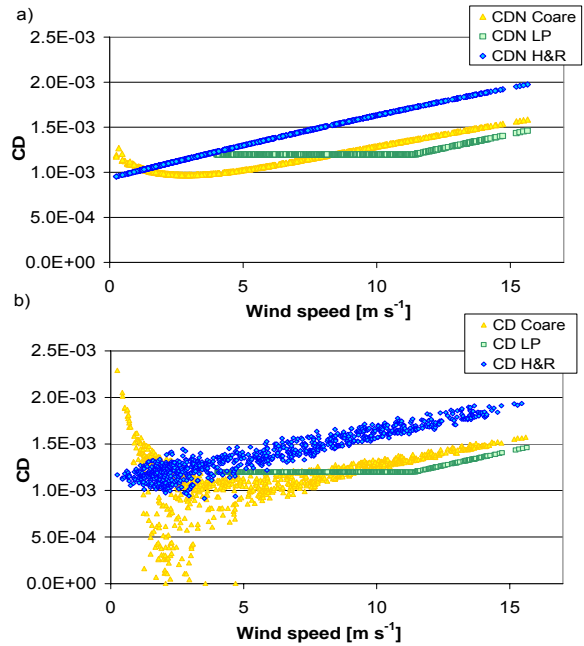


Fig. 2. a) Neutral drag coefficient, b) Non-neutral drag coefficient computed from TC, LP and HR formulas.

Table 1. Neutral and non neutral drag coefficients computed from TC, LP and HR formulas for buoys D090, 46023, 46054 and 46062

Measurement buoy	Wind speed [m s ⁻¹]	Drag coefficient from TC algorithm	Neutral drag coefficient from TC algorithm	Drag coefficient from LP formula	Drag coefficient from HR formula	Neutral drag coefficient from HR formula	
D090	AVERAGE	5.89	1.140E-03	1.128E-03	1.211E-03	1.318E-03	1.355E-03
	STD. DEV	3.92	2.966E-04	1.611E-04	3.820E-05	3.272E-04	2.685E-04
	MEDIAN	5.18	1.175E-03	1.058E-03	1.200E-03	1.303E-03	1.315E-03
46023	AVERAGE	6.23	1.102E-03	1.121E-03	1.201E-03	1.344E-03	1.396E-03
	STD. DEV	2.76	2.460E-04	1.167E-04	6.700E-06	2.067E-04	1.968E-04
	MEDIAN	6.3	1.146E-03	1.102E-03	1.200E-03	1.352E-03	1.406E-03
46054	AVERAGE	8.09	1.146E-03	1.214E-03	1.217E-03	1.514E-03	1.524E-03
	STD. DEV	3.36	2.975E-04	1.520E-04	3.940E-05	2.417E-04	2.346E-04
	MEDIAN	8.6	1.215E-03	1.226E-03	1.200E-03	1.553E-03	1.566E-03
46062	AVERAGE	5.9	3.288E-03	1.115E-03	1.203E-03	1.321E-03	1.372E-03
	STD. DEV	3.03	4.688E-04	1.292E-04	1.750E-05	2.303E-04	2.152E-04
	MEDIAN	5.69	1.139E-03	1.078E-03	1.200E-03	1.309E-03	1.362E-03

As can be seen in Fig. 2a, even the neutral drag coefficient exhibits significant difference among the analyzed schemes. The smallest range of the neutral drag coefficient ($1.2 \cdot 10^{-3}$ - $1.5 \cdot 10^{-3}$) is provided by the LP formula. This is a consequence of the specifics of the algorithm, which for wind speeds below 11 m s^{-1} provides a constant drag coefficient, and for the wind speed above this range treats the drag coefficient as linearly increasing with the wind speed.

The neutral drag coefficient obtained from the HR formula exhibits the highest variability among the analyzed schemes (from $0.9 \cdot 10^{-3}$ to $2 \cdot 10^{-3}$), and exhibits a nearly linear increase with the wind speed for the entire wind speed range. The calibration of constants in the HR formula (Eq. 2) causes that for neutral conditions; at wind speed around 4 m s^{-1} the HR and LP formulas give similar results. However, for higher wind speeds the HR scheme provides a higher drag coefficient (and wind stress) than the LP formula, and the difference between them increases with the wind speed up to 11 m s^{-1} , where LP starts to operate in the mode of the wind speed dependence. The range of the TC neutral drag coefficient ($0.9 \cdot 10^{-3}$ to $1.6 \cdot 10^{-3}$) is broader than that observed for LP formula, but evidently narrower than for HR scheme.

The neutral drag coefficient is computed by the TC algorithm under the assumption of a logarithmic wind speed profile with stability correction function ψ_u equal to zero:

$$U_{wg} = \frac{U_*}{\kappa} \cdot \left[\ln \left(\frac{z}{z_0} \right) - \psi_u \left(\frac{z}{L} \right) \right] \quad (5)$$

where U_{wg} is the wind speed at the height z corrected by the gustiness, U_* is the friction velocity, z_0 is the roughness length, κ is von Kármán constant (0.4), ψ_u is the stability correction function for the wind speed, and L is the Monin-Obukhov length. The relationship between the roughness length and the friction velocity used in the TC iterative process is given by the following equation:

$$z_0 = \frac{\alpha_c \cdot U_*^2}{g} + 0.11 \frac{\nu}{U_*} \quad (6)$$

where α_c is Charnock constant, U_* is the friction velocity, g is the gravitational acceleration and ν is the kinematic viscosity. The first term contributes to the roughness length for high wind speeds (aerodynamically rough flow), whereas the second contributes for low wind speeds (aerodynamically smooth flow). As a consequence, the neutral drag coefficient (which is proportional to the square of the friction velocity), decreases with the wind speed, reaches a minimum at 3 m s^{-1} and increases for the higher wind speeds. Because of this, for the lowest wind speeds (below 1.5 m s^{-1}), the TC algorithm provides significantly higher drag coefficient than the HR formula. For the higher wind speeds (up to 8 m s^{-1}), the drag coefficient computed from the TC algorithm is smaller than that from the HR and LP formulas. However, for higher wind speeds (above 8 m s^{-1}), the TC results are between these obtained from the LP and HR formulas. The minimum, the maximum, and the median of the neutral drag coefficient computed from the analyzed algorithms are presented in Table. 1.

Notice that for buoys 46023 and 46062, which experienced relatively high wind speeds, the differences between the results of TC and HR do not exceed 2%. For the lower wind speeds observed by buoys D090 and 46062 the difference between these two drag coefficients can reach 10%. The drag coefficient computed with stability corrections is shown in Fig. 2b. The effect of the stability correction on the computed drag coefficient is the most evident for the TC algorithm. Notice that the range of the non-neutral drag coefficient is broadest for the TC algorithm due to the high variability of the low wind speeds (below 4 m s^{-1}). With the HR formula, the discrepancies between the neutral and non-neutral computations are also most significant for the low wind speed regime. However, the effect of stability correction on the HR formula is much more

uniform and can be observed for the low and the high wind speeds as well (see the discussion in Section 4.3).

4.2 Influence of the input parameters on the computed wind stress

A series of sensitivity tests has been performed to evaluate the effect of various input parameters on the wind stress computed from HR and TC schemes. For the input parameters we chose the average values of the sea surface and air temperatures and shortwave (SWF) and longwave (LWF) radiation fluxes measured by buoy D090 during the period from 28 June to 4 August 2001 (LWF = 150 W m^{-2} , SWF = 250 W m^{-2} , RH = 92%, $T_s = 12^\circ\text{C}$). Sensitivity tests were performed in such a way that one analyzed parameter could be varied while all other parameters were kept constant. The computations for each analyzed parameter were repeated for various wind speeds from 0 to 15 m s^{-1} , to obtain also information about the wind speed conditions at which the influence of the analyzed parameter is the most significant.

4.3 Effect of the atmospheric stability on the computed wind stress

The implementation of stability corrections reduces the discrepancies between analyzed schemes (see the values of neutral and non-neutral drag coefficient for the HR and TC formulas presented in Table 1). One should bear in mind that the drag coefficient computed from the TC algorithm is corrected not only due to the sea-air temperature difference but also due to effects of the warm oceanic upper layer, the cool-skin surface temperature correction, and the humidity. Since observed change of the drag coefficient is a joint effect, it cannot be directly interpreted as the exclusive effect of the atmospheric stability.

In order to separate the effect of atmospheric stability, a special set of sensitivity tests was performed using air temperature from 7 to 15°C , and wind speed from 1 to 10 m s^{-1} . Results obtained from the HR and TC schemes are presented in Fig.3.

The stability influence on the drag coefficient (and the wind stress) computed from the HR formula differ significantly from the stability influence on the TC algorithm. In the HR formula (Eq. 2), the highest contribution (and the only dependence on the sign of sea-air temperature difference) comes from the third term. The fifth and sixth terms introduce only small modifications that gradually reduce the stability influence with the increasing of the wind speed. As a consequence, an increase of the stability causes an increase of the drag coefficient with a slightly stronger effect for low than for high winds. The drag coefficient computed from the TC algorithm is affected by the stability in the opposite way. The drag coefficient decreases with the increasing stability. This behavior seems to be in agreement with the physical explanation of the processes taking a place at the interface. Notice that stable conditions, with the sea surface colder than the air, inhibit vertical momentum transfer from the air to

the sea. On the other hand, unstable conditions (sea surface warmer than the air) promote additional mixing due to the buoyancy effect, and intensify momentum transfer (the wind stress). Note that in the case of the TC algorithm (unlike the HR formula) the effect of stability rapidly decreases with the increase in wind speed. For low wind speeds, and near neutral conditions, even a small change in the stability causes a very significant change in the drag coefficient. The observed effect is an implication of Eq. (6), which shows that in a low wind speed regime the friction velocity and the scale temperature parameter act in opposite directions causing significant change in the Monin-Obukhov length and consequently the value of the stability correction function Ψ_u , which influences the wind profile (Eq. 5) and consequently the wind stress.

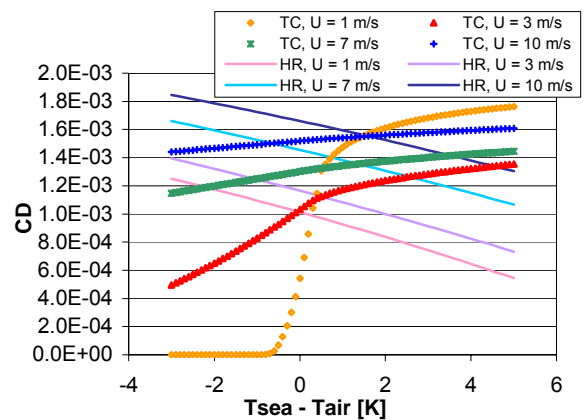


Fig. 3. Drag coefficient from TC and HR formulas, as a function of difference between sea and air temperatures for various wind speeds.

4.4 Other parameters influencing the wind stress

In the TC algorithm, other parameters besides the atmospheric stability also act on the wind stress. Since this algorithm takes into account not only the heat and momentum flux, but also the water vapor flux, the water content in the air strongly influences the computed drag coefficient. The results of drag coefficient computations performed for various relative humidities are presented in Fig. 4.

As can be noticed, the highest variability of the drag coefficient due to humidity corresponds to the wind speed below 4 m s^{-1} . In this range, a relatively small change of relative humidity causes a very significant change in the drag coefficient. For relative humidity below 80%, the drag coefficient increases with the wind speed; however, humidity above 84% completely changes this characteristic, causing a dramatic decrease of the drag coefficient for weak winds.

The same type of drag coefficient variability can be observed in Fig. 2b where for low wind speeds the variability of the drag coefficient computed from the TC algorithm is the greatest. The main reason for that is the humidity correction included in the virtual temperature.

For close to neutral conditions, this correction can change the TC stability regime from unstable to stable, causing a dramatic decrease in the drag coefficient as presented in Fig. 4.

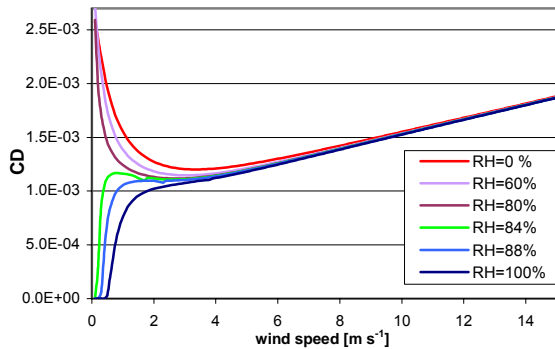


Fig. 4. Drag coefficient computed from TC algorithm as a function of wind speed for the relative humidities from 0 to 100%, and the wind speed from 0 to 15 m s^{-1} .

5. ANALYSIS OF THE WIND STRESS CURL COMPUTED FROM VARIOUS SCHEMES

The wind stress curl has been computed using the wind stress components calculated for the set of three closely separated buoys as presented in Section 3.3. The results of the wind stress curl computations for the LP, HR and TC formulas are presented in Fig.5a.

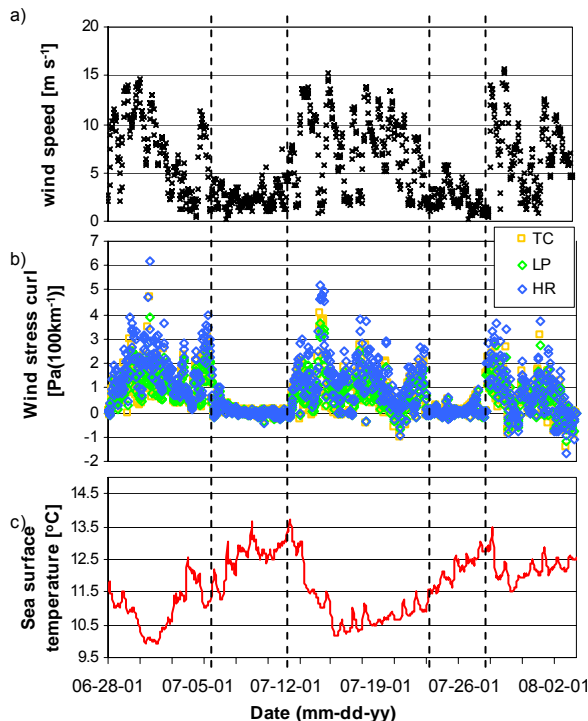


Fig. 5. Intercomparison of the a) wind speed measured by buoy D090, b) The wind stress curl computed from TOGA Coare, Large and Pond, and Hellerman and Rosenstein algorithms, c) Sea-surface temperature measured by buoy D090).

Most of the time the computed wind stress curl is mostly positive for all wind stress parameterizations; however differences among average wind stress curl for the different schemes can reach as high as 39%. The highest values of the curl were obtained using the HR formula (median value of $0.70 \text{ Pa}\cdot(100 \text{ km})^{-1}$), computations performed on the basis of the TC algorithm provided a median value around $0.47 \text{ Pa}\cdot(100 \text{ km})^{-1}$, whereas the median of the curl calculated using the LP formula reached a value of $0.44 \text{ Pa}\cdot(100 \text{ km})^{-1}$.

Wind stress curl is computed on the basis of differences in wind stress components (Eq. 4) for the buoy locations indicated in Fig. 1.

The strong influence of the wind speed on the wind stress (second power), reduces the absolute variability of wind stress for low wind speeds, and enhances it in a regime of high wind stress. Consequently, the scheme providing the highest drag coefficient variability for relatively strong winds provides also the highest wind stress curl.

The negative wind stress curl occurs mostly for low winds, whereas greater wind speeds favor positive wind stress curl. As a consequence, a scheme which provides high variability of wind stress for lower wind speeds will promote negative curl, whereas a scheme which provides higher variability for higher winds promotes positive curl. That is the reason why the HR formula promotes positive curl, whereas the TC algorithm promotes negative.

6. EFFECT OF THE WIND STRESS AND THE WIND STRESS CURL ON THE SST

Figure 5 shows the relationship between the SST and the wind stress curl as computed by the three analyzed algorithms. As can be noticed, all schemes show a significant trend of decreasing SST for increasing wind stress curl. The maximum of the wind stress curl (present at the beginning of the analyzed period) corresponds to a minimum of the sea surface temperature. The following relaxation period with the very low wind stress curl (vertical dashed line in Fig. 5) and the change of the sign of the wind stress curl from positive to negative (indicating the change of the wind stress rotation from counterclockwise to clockwise) reflects the sea surface temperature, causing its increase from 10°C to 13.5°C .

Wind stress curl fluctuations also have a big influence on the sea surface temperature with evident cooling of the sea surface during positive wind stress curl and warming during negative curl and relaxation periods.

This relationship between the wind stress curl and the sea surface temperature is strongly correlated to the upwelling and downwelling as described by Enriquez and Friehe (1995). However, one should bear in mind that the observed SST variation can be a joint effect of

the upwelling induced by the wind stress curl and by the along-shore component of the wind stress as well.

7. CONCLUSIONS

The results obtained show that significant discrepancies exist between schemes for the wind stress, as well as for the wind stress curl. For low wind speeds (below 3 m s^{-1}), stability and humidity corrections implemented in the TC algorithm cause very high variability in the drag coefficient, which can vary from close to 0 up to $2.3 \cdot 10^{-3}$. Except for the lowest wind speed regime (where the variation of the TC drag coefficient is very high), the HR formula provides the greatest wind stress. For greater wind speeds (but less than 8 m s^{-1}) the wind stress computed from LP is higher than that obtained from TC. For wind speeds above 8 m s^{-1} , the situation reverses, and LP provides the smallest values of the wind stress.

Differences in the computed wind stress affect the variation of the wind stress curl. The highest values of the wind stress curl were obtained from the HR scheme, since it provides the highest variations of the wind stress for high wind speeds. The wind stress curl computed from the TC algorithm is smaller, and that obtained from the most uniform LP formula is the smallest. The characteristics of stability corrections implemented in the analyzed algorithms cause the TC algorithm to promote negative wind stress curl, whereas HR induces positive wind stress curl. Despite observed differences, for all analyzed schemes the wind stress curl computed on the basis of spatial wind stress distribution is correlated to SST. During periods of positive curl (usually 7 to 9 days), the SST decreases (upwelling), whereas during relaxation periods and events of negative curl (usually 5 to 7 days) the sea surface warms up.

REFERENCES

- Bignami, F., Marullo, S., Santoleri, R., Schiano, M.E., 1995: Longwave radiation budget in the Mediterranean Sea. *J. Geophys. Res.*, **100 (C2)**, 2501-2514, 1995.
- Dorman, C.E., Holt, T., Rogers, D.P., & Edwards, K.A. (2000). Large-scale structure of the June-July 1996 marine boundary layer along California and Oregon. *Mon. Wea. Rev.*, **128**, 1632-1652.
- Enriquez, A. G. and C. A. Friehe, 1995: Effects of wind stress and wind stress curl variability on coastal upwelling. *J. Phys. Ocean.*, **25**, 1651-1671.
- Hellerman, S., and M. Rosenstein, 1983: Normal monthly wind stress over the world ocean with error estimates. *J. Phys. Ocean.*, **13**, 1093-1104.
- Fairall, C. W., E. F. Bradley, D. P. Rogers, J. B. Edson, and G. S. Young, 1996: Bulk parameterization of air-sea fluxes for Tropical Ocean Global Atmosphere Coupled Ocean-Atmosphere Response Experiment. *J. Geophys. Res.*, **101**, 3747-3764.
- Jin, X., X. Zhang and T. Zhou, 1999, Fundamental framework and experiments of the third generation of IAP/LASG world ocean general circulation model. *Adv. Atmos. Sci.*, **16**, 197-215.
- Koracin, D., C. E. Dorman, and E. P. Dever, 2004: Coastal perturbations of marine layer winds, wind stress, and wind stress curl along California and Baja California in June 1999. *J. Phys. Ocean.*, **34**, 1152-1173.
- Large, W. G., and S. Pond, 1981: Open ocean momentum flux measurements in moderate to strong winds. *J. Phys. Ocean.*, **11**, 324-481.
- Metzger, E. J., 2003: Upper ocean sensitivity to wind forcing in the South China Sea. *J. Ocean.*, **59** (No. 6), 783-798.
- Rosati, A., and K. Miyakoda, 1988: A general circulation model for the upper ocean circulation. *J. Phys. Ocean.*, **18**, 1601-1626.
- Roussenov, V. E. Stanev, V. Artale and N. Pinardi, 1995: A seasonal model of the Mediterranean Sea. *J. Geophys. Res.*, **100, C7**, 13515-13538.
- Samelson, R. M., P. Barbour, J. Barth, S. Bielli, T. Boyd, D. Chelton, P. Kosro, M. Levine, E. Skillingstad, and J. Wilczak, 2002: Wind stress forcing of the Oregon coastal ocean during the 1999 upwelling season. *J. Geophys. Res.*, **107**, doi:10.1029/2001JC000900.